

A Search for New Exotic Particles with Jets in Proton-Proton Collisions at the CMS Experiment

Dissertation

zur

**Erlangung der naturwissenschaftlichen Doktorwürde
(Dr. sc. nat.)**

vorgelegt der

Mathematisch-naturwissenschaftlichen Fakultät

der

Universität Zürich

von

Johnny B. Goode

aus

Deutschland

Promotionskommission

Prof. Dr. Ben Kilminster (Vorsitz)

Prof. Dr. Florencia Canelli

Prof. Dr. Nicola Serra

Prof. Dr. Gino Isidori

Zürich, 20...

2 Abstract

3 The Standard Model of particle physics has been very successful. But there are problems. They
4 can be explained by new exotic particles.

5 A search is presented for a new exotic particle. Events with jets are considered. A novel
6 technique is used. The search is based on Run-2 proton-proton collision data at a center-of-mass
7 energy of 13 TeV recorded with the CMS detector corresponding to an integrated luminosity of
8 137.1 fb^{-1} .

9 Upper limits are set on the production cross section of a new exotic particle as a function of
10 mass. Results are compared with theoretical predictions to obtain lower limits on the mass. At
11 95% confidence level, new exotic particles are excluded for masses below X GeV.

¹³ **Acknowledgements**

¹⁴ I want to thank the great people in the UZH group and at CMS Collaboration that have helped
¹⁵ me along the way, and with whom it was a great privilege and pleasure to work on diverse
¹⁶ projects and push the limits of our understanding of Nature.

¹⁷ Special thanks go to my supervisor, Prof. Dr. ...; my supervisor Dr. ...; ...

¹⁸ I would also like to thank my parents and family, for supporting me along my studies.

Contents

20	1 Introduction	1
21	2 The Standard Model	2
22	2.1 The Standard Model	2
23	2.1.1 The Standard Model Lagrangian	2
24	2.1.2 The gauge sector	2
25	2.1.3 The Yukawa sector	5
26	2.1.4 CKM matrix	5
27	2.2 Higgs	6
28	2.3 The physics of proton-proton collisions	6
29	3 Beyond the Standard Model	8
30	4 The CMS Experiment	10
31	4.1 The Large Hadron Collider	10
32	4.1.1 Luminosity	10
33	4.2 The CMS detector	12
34	4.2.1 Coordinate system	13
35	4.2.2 The solenoid magnet & flux-return yoke	13
36	4.2.3 The pixel tracker	13
37	4.2.4 The silicon strip tracker	13
38	4.2.5 The electromagnetic calorimeter	13
39	4.2.6 The hadronic calorimeter	13
40	4.2.7 The muon system	13
41	4.2.8 The trigger system	15
42	5 Object & Event Reconstruction	16
43	5.1 Principles of particle identification	16
44	5.2 Particle-flow algorithm	16
45	5.3 Primary vertex	16
46	5.4 Electrons	16
47	5.5 Muons	16
48	5.6 Hadronically Decayed τ Leptons	18
49	5.7 Jets	18
50	5.8 Bottom quark identification	18
51	5.9 Missing transverse energy	20
52	6 Data sets & Simulated Samples	21
53	6.1 Data sets	21
54	6.2 Event simulation	21

55	6.3 Backgrounds	21
56	6.3.1 Simulated backgrounds	21
57	6.3.2 Cross sections	24
58	7 Event Selection	25
59	References	26

60 1 Introduction

61 Over the last 100 years, physicists have made large strides in understanding the natural laws
62 that govern the universe as we know it. The Standard Model (SM) of particle physics describes
63 matter and its interactions.

64 In 2012, the discovery of the Higgs boson was announced by the ATLAS and CMS experiments [1–3] at CERN’s LHC. The Higgs was 47 years before that [4, 5]. Despite its many
65 successes, there are both theoretical and experimental reasons that imply the SM is not the final
66 theory of Nature.

67 This dissertation has the following structure: Chapter 2 discusses the SM, after which Chapter
68 3 motivates the search for new hypothetical particles. Chapter 4 describes the LHC accelerator,
69 CMS detector and the data collection. Chapter 5 describes the physics objects that are
70 relevant for this thesis. After these, Chapter 7 discusses the selections.

72 2 The Standard Model

73 This chapter introduces the Standard Model (SM) of particle physics. I left a bit of text with
74 equations, citations, figures, and tables as an example of this template.

75 2.1 The Standard Model

76 A rough timeline of the experimental discovery of particles is given by Fig. 2.1. More detailed
77 historical discussions can be found in Refs. [6–8].

78 With a mass of $m_t \approx 172.8 \text{ GeV}$ [10, p. 32], the top quark is by far the heaviest fermion.

79 The discovery of the Higgs was announced in 2012 [1–3, 11]. A single Higgs boson is the
80 simplest and most minimal solution, although it is possible to achieve SBB with more than one
81 Higgs boson. No evidence of additional Higgs bosons have been found so far [12].

82 2.1.1 The Standard Model Lagrangian

83 The SM is encoded in the *SM Lagrangian density*. The terms of the Lagrangian density can be
84 grouped into three separate *sectors*:

$$\mathcal{L}_{\text{SM}} = \mathcal{L}_{\text{gauge}} + \mathcal{L}_{\text{Higgs}} + \mathcal{L}_{\text{Yukawa}}. \quad (2.1)$$

85 Secondly, the SM is a *gauge theory*: It has an internal symmetry that corresponds to the
86 local $\text{SU}(3)_C \times \text{SU}(2)_L \times \text{U}(1)_Y$ symmetry group. The SM gauge group is spontaneously broken
87 to

$$\text{SU}(3)_C \times \text{SU}(2)_L \times \text{U}(1)_Y \xrightarrow{\text{SSB}} \text{SU}(3)_C \times \text{U}(1)_{\text{EM}} \quad (2.2)$$

88 by the nonzero vev of the Higgs field, where $\text{U}(1)_{\text{EM}}$ is the gauge symmetry group for QED.

89 2.1.2 The gauge sector

The gauge sector can be written as

$$\mathcal{L}_{\text{gauge}} = \sum_f \sum_{\psi_f} \bar{\psi}_f i\gamma^\mu D_\mu \psi_f - \frac{1}{4} G_{\mu\nu}^a G_a^{\mu\nu} - \frac{1}{4} W_{\mu\nu}^i W_i^{\mu\nu} - \frac{1}{4} B^{\mu\nu} B^{\mu\nu}, \quad (2.3)$$

90 in natural units $c = \hbar = 1$ [15], and where $a = 1, \dots, 8$ and $i = 1, 2, 3$. In the first term, matter
91 is given by five fermion fields ψ_f in three generations $f = 1, 2, 3$;

$$Q_L^f = \begin{pmatrix} u_L^f \\ d_L^f \end{pmatrix}, \quad u_R^f, \quad d_R^f, \quad L_L^f = \begin{pmatrix} \nu_L^f \\ e_L^f \end{pmatrix}, \quad e_R^f. \quad (2.4)$$

92 Their Dirac adjoints are given by $\bar{\psi}_f = \psi_f^\dagger \gamma^0$.

93 The covariant derivative

$$D_\mu = \partial_\mu + ig_s t_a G_\mu^a + ig T_i W_\mu^i + ig' \frac{Y}{2} B_\mu \quad (2.5)$$

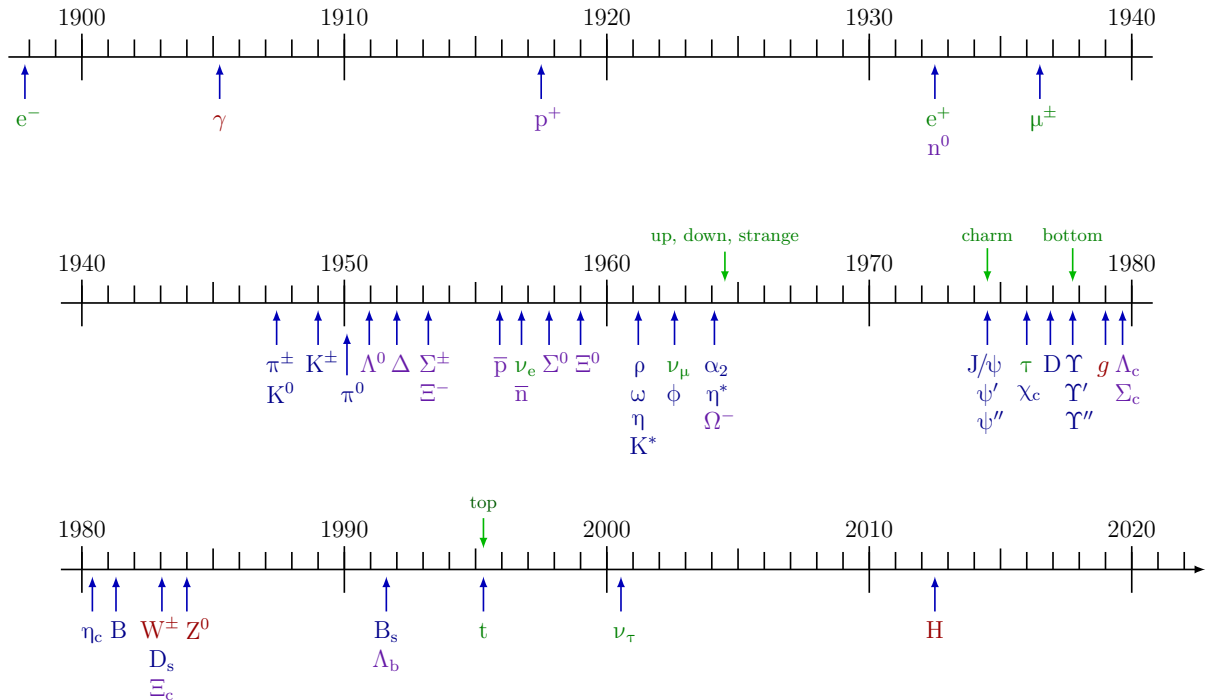


Figure 2.1: A timeline of particle physics in the last 130 years. Adapted from Ref. [9].

three generations of matter (fermions)			interactions / forces (bosons)	
I	II	III	g	H
mass charge spin	$\simeq 2.2 \text{ MeV}$ $+2/3$ $1/2$ u up	$\simeq 1.3 \text{ GeV}$ $+2/3$ $1/2$ c charm	$\simeq 173 \text{ GeV}$ $+2/3$ $1/2$ t top	0 0 1 g gluon
QUARKS	$\simeq 4.7 \text{ MeV}$ $-1/3$ $1/2$ d down	$\simeq 96 \text{ MeV}$ $-1/3$ $1/2$ s strange	$\simeq 4.2 \text{ GeV}$ $-1/3$ $1/2$ b bottom	0 0 1 γ photon
LEPTONS	$\simeq 0.511 \text{ MeV}$ -1 $1/2$ e electron	$\simeq 106 \text{ MeV}$ -1 $1/2$ μ muon	$\simeq 1.777 \text{ GeV}$ -1 $1/2$ τ tau	$\simeq 80.4 \text{ GeV}$ ± 1 1 W W boson
	$< 1.0 \text{ eV}$ 0 $1/2$ ν_e electron neutrino	$< 0.17 \text{ eV}$ 0 $1/2$ ν_μ muon neutrino	$< 18.2 \text{ MeV}$ 0 $1/2$ ν_τ tau neutrino	$\simeq 91.2 \text{ GeV}$ 0 1 Z Z boson
SCALAR BOSONS				
GAUGE BOSONS VECTOR BOSONS				

Figure 2.2: A table of the particles in Standard Model of particle physics and their properties. Figure adapted from Refs. [13] and [14].

Table 2.1: Summary of the representation and quantum numbers SM fields. Bold numbers indicate the dimension of the representation under the respective gauge group.

Field name	Symbol	Representations		Quantum numbers		
		SU(3) _C	SU(2) _L	T_3	$Y/2$	$Q = T_3 + Y/2$
Quark doublet	$Q_L = \begin{pmatrix} u_L \\ d_L \end{pmatrix}$	3	2	$\begin{pmatrix} +\frac{1}{2} \\ -\frac{1}{2} \end{pmatrix}$	$+\frac{1}{6}$	$\begin{pmatrix} +\frac{2}{3} \\ -\frac{1}{3} \end{pmatrix}$
Up-quark singlet	u_R	3	1	$+\frac{2}{3}$	$+\frac{2}{3}$	$+\frac{2}{3}$
Down-quark singlet	d_R	3	1	$-\frac{1}{3}$	$-\frac{1}{3}$	$-\frac{2}{3}$
Lepton doublet	$L_L = \begin{pmatrix} \nu_L \\ e_L \end{pmatrix}$	1	2	$\begin{pmatrix} +\frac{1}{2} \\ -\frac{1}{2} \end{pmatrix}$	$-\frac{1}{2}$	$\begin{pmatrix} 0 \\ -1 \end{pmatrix}$
Lepton singlet	e_R	1	1	0	-1	-1
Gluon field	G_μ^a	8	1	0	0	0
Weak gauge field	$W_\mu^i = \begin{pmatrix} W_\mu^+ \\ W_\mu^- \\ W_\mu^3 \end{pmatrix}$	1	3	$\begin{pmatrix} +1 \\ -1 \\ 0 \end{pmatrix}$	0	$\begin{pmatrix} +1 \\ -1 \\ 0 \end{pmatrix}$
Hypercharge field	B_μ	1	1	0	0	0
Higgs doublet	$\Phi = \begin{pmatrix} \phi^+ \\ \phi^0 \end{pmatrix}$	1	2	$\begin{pmatrix} +\frac{1}{2} \\ -\frac{1}{2} \end{pmatrix}$	$+\frac{1}{2}$	$\begin{pmatrix} +1 \\ 0 \end{pmatrix}$
Conjugate Higgs doublet	$\Phi^c = \begin{pmatrix} \phi^{0*} \\ \phi^- \end{pmatrix}$	1	2	$\begin{pmatrix} +\frac{1}{2} \\ -\frac{1}{2} \end{pmatrix}$	$-\frac{1}{2}$	$\begin{pmatrix} 0 \\ -1 \end{pmatrix}$

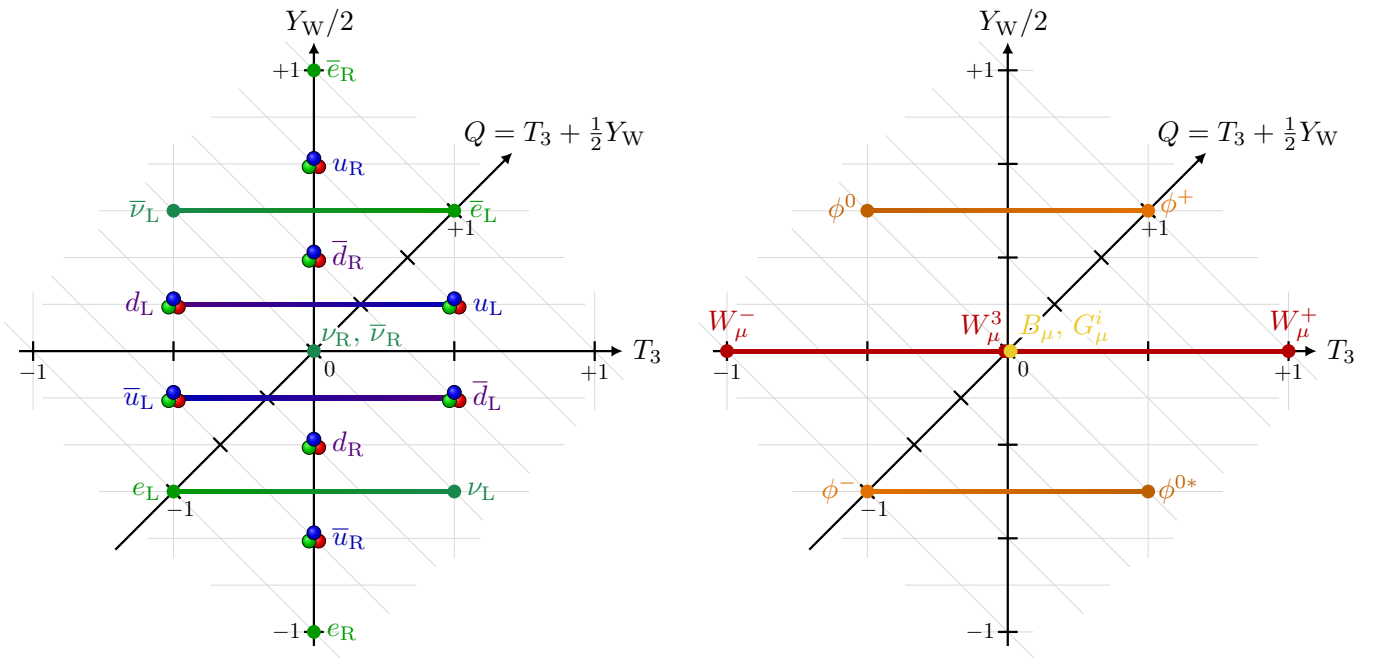


Figure 2.3: Graph of the $(T_3, Y/2)$ quantum numbers. Adapted from Ref. [16].

where T_i and t_a are the generators for $SU(2)_L$ and $SU(3)_C$, respectively, and Y is the weak hypercharge of the field that D_μ acts on.

Through the Higgs mechanism, the gauge bosons acquire mass and mix into the mass eigenstates

$$W_\mu^\pm = \frac{W_\mu^1 \mp iW_\mu^2}{\sqrt{2}}, \quad Z_\mu = W_\mu^3 \cos \theta_W + B_\mu^3 \sin \theta_W, \quad A_\mu = W_\mu^3 \sin \theta_W - B_\mu^3 \cos \theta_W, \quad (2.6)$$

where W_μ^\pm are the charged W boson fields, Z_μ is the neutral Z boson field, A_μ is the photon field, and θ_W is the Weinberg angle given by $\sin \theta_W = g'/\sqrt{g^2 + g'^2}$. After mixing, the new covariant derivative becomes

$$D_\mu = \partial_\mu + ig_s t_a G_\mu^a + i \frac{g}{\sqrt{2}} T^+ W_\mu^+ + i \frac{g}{\sqrt{2}} T^- W_\mu^- + i \frac{g}{\cos \theta_W} (T_3 - \sin^2 \theta_W Q) Z_\mu + ieQ A_\mu, \quad (2.7)$$

with ladder operators $T^\pm = T_1 \pm iT_2$.

2.1.3 The Yukawa sector

In order to explain mass of the fermions,

$$\mathcal{L}_{\text{Yukawa}} = -Y_d^{fg} \bar{Q}_L^f \Phi d_R^g - Y_u^{fg} \bar{Q}_L^f \Phi^c u_R^g - Y_e^{fg} \bar{L}_L^f \Phi e_R^g + \text{h.c.}, \quad (2.8)$$

with the conjugate Higgs doublet $\Phi^c = i\sigma_2 \Phi^\dagger$, and unitary Yukawa matrices Y_d^{fg} , Y_u^{fg} , $Y_e^{fg} \in U(3)$ that mixes the fermion generations. As Φ is a scalar field that forms a weak isospin doublet,

$$\Phi = \begin{pmatrix} \phi^+ \\ \phi^0 \end{pmatrix}. \quad (2.9)$$

Because the Higgs vev is nonzero, we can fix the $SU(2)_L$ gauge. It is convenient to choose the unitary gauge

$$\Phi = \frac{1}{\sqrt{2}} \begin{pmatrix} 0 \\ v + h \end{pmatrix}, \quad (2.10)$$

with the vev $v \approx 246$ GeV, a real constant, and the neutral Higgs field h , a (real) scalar. Therefore, after SSB, we are left with

$$\mathcal{L}_{\text{Yukawa}} = -\frac{Y_d^{fg}}{\sqrt{2}} \bar{d}_L^f (v + h) d_R^g - \frac{Y_u^{fg}}{\sqrt{2}} \bar{u}_L^f (v + h) u_R^g - \frac{Y_e^{fg}}{\sqrt{2}} \bar{e}_L^f (v + h) e_R^g + \text{h.c.} \quad (2.11)$$

2.1.4 CKM matrix

To explain the suppressed decay rate of $K^0 \rightarrow \mu^+ \mu^-$, Glashow, Iliopoulos, and Maiani used a mixing matrix and proposed the existence of the charm quark [17]. This is referred to as the *Glashow–Iliopoulos–Maiani (GIM) mechanism*. The mixing of two quark generations is given by the *Cabibbo matrix*:

$$\begin{pmatrix} d' \\ s' \end{pmatrix} = \begin{pmatrix} \cos \theta_C & \sin \theta_C \\ -\sin \theta_C & \cos \theta_C \end{pmatrix} \begin{pmatrix} d \\ s \end{pmatrix}, \quad (2.12)$$

where $|d'\rangle$ and $|s'\rangle$ represent the weak eigenstates, which are linear combinations of the mass eigenstates $|d\rangle$ and $|s\rangle$. The mixing is quantified with the *Cabibbo angle* $\theta_C \approx 13.04^\circ$.

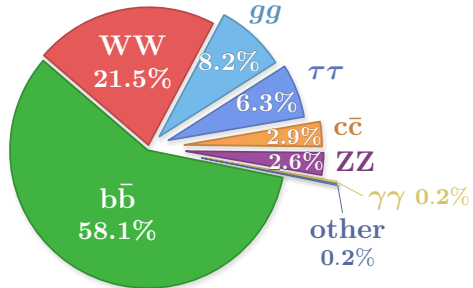


Figure 2.4: Pie chart of Higgs branching fractions. Adapted from Ref. [18].

The mixing of three generations is given by

$$\begin{pmatrix} d' \\ s' \\ b' \end{pmatrix} = \begin{pmatrix} V_{ud} & V_{us} & V_{ub} \\ V_{cd} & V_{cs} & V_{cb} \\ V_{td} & V_{ts} & V_{tb} \end{pmatrix} \begin{pmatrix} d \\ s \\ b \end{pmatrix}, \quad (2.13)$$

where the matrix is the so-called *Cabbibo-Kobayashi-Maskawa (CKM) matrix*, denoted by V_{CKM} .

2.2 Higgs

A pie chart of Higgs decay can be found in Fig. 2.4.

2.3 The physics of proton-proton collisions

The substructure of the proton has been carefully studied in deep inelastic scattering (DIS) experiments at SLAC [19, 20] and DESY [21], which collided electrons or positrons with protons.

In the parton model, *parton distribution functions* (PDFs) describe the probability of finding a parton of type p with momentum fraction x in a collision at some momentum scale Q as a function of the form $f_p(x, Q^2)$ [22–26]. The proton has *valence quarks* and *sea quarks*. To reflect the proton quantum numbers, the PDFs are normalized:

$$\int_0^1 [f_u(x, Q^2) - f_{\bar{u}}(x, Q^2)] dx = 2, \quad \int_0^1 [f_d(x, Q^2) - f_{\bar{d}}(x, Q^2)] dx = 1. \quad (2.14)$$

This follows from the factorization theorem [28, 29], which provides a formula to calculate the cross sections of a hard process with an integral of the form

$$\sigma(\text{pp} \rightarrow X + Y) = \sum_{i,j} \int_0^1 \int_0^1 f_i(x_1, Q^2) f_j(x_2, Q^2) \hat{\sigma}_{ij \rightarrow X}(x_1, x_2, Q^2) dx_1 dx_2, \quad (2.15)$$

where $\hat{\sigma}_{ij \rightarrow X}(x_1, x_2, Q^2)$ is the parton-level cross section of the hard process, $i + j \rightarrow X$, and parton i (j) carries a fraction x_1 (x_2) of the momentum of its mother proton.

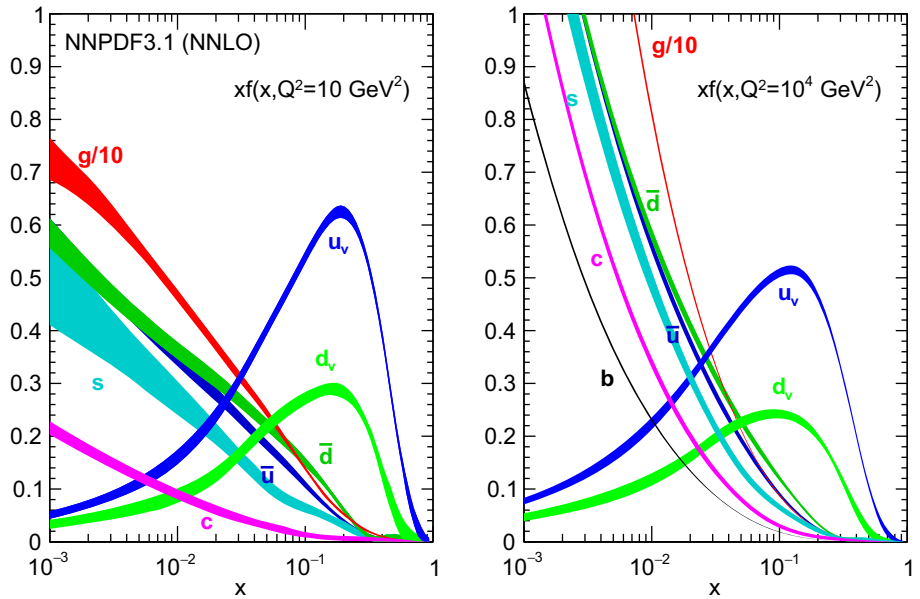


Figure 2.5: Plot of the proton PDF $f_p(x, Q^2)$ times the momentum fraction x as calculated by NNPDF3.1 at NNLO accuracy in perturbation theory for $Q^2 = 10 \text{ GeV}^2$ (left) and $Q^2 = 10^4 \text{ GeV}^2$ (right). Adapted from [27].

¹³² **3 Beyond the Standard Model**

¹³³ The SM of particle physics is successful. Fine-structure constant $\alpha = e^2/4\pi$ has been precisely
¹³⁴ calculated and measured [30–33]. In 2012, the discovery of the Higgs boson was announced by
¹³⁵ the ATLAS and CMS experiments at the CERN LHC [1–3, 11], more than 47 years after its
¹³⁶ prediction [4, 5]. But there are both problems. The following section highlights several examples
¹³⁷ of open questions in physics.

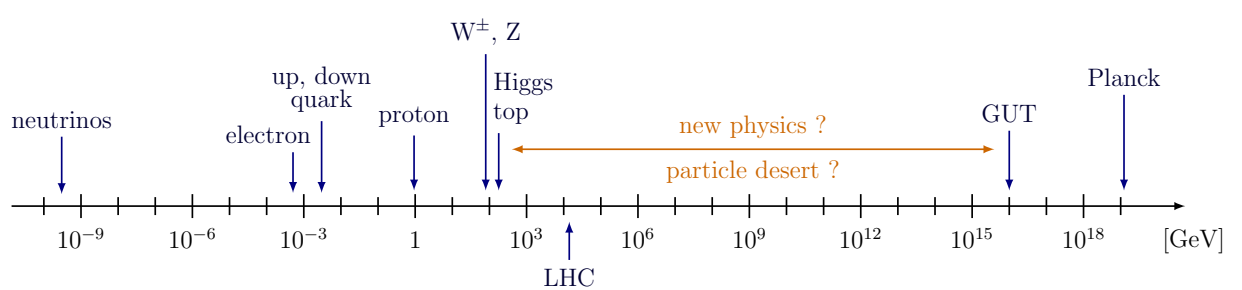


Figure 3.1: Logarithmic scale of different energy scales in particle physics. Adapted from Ref. [9].

¹³⁸ 4 The CMS Experiment

¹³⁹ This chapter will discuss the experimental setup.

¹⁴⁰ 4.1 The Large Hadron Collider

¹⁴¹ The Large Hadron Collider (LHC) is the world's largest and most powerful particle collider
¹⁴² with a 27 km circumference and a record collision energy of 13.6 TeV. It surpasses the Tevatron
¹⁴³ accelerator at Fermilab in the United States [35] (6.3 km, 1.96 TeV), and LEP (209 GeV) [10,
¹⁴⁴ Section 32].

¹⁴⁵ During the data-taking period of 2015 to 2018, referred to as "Run 2", the energy of each
¹⁴⁶ proton beam was 6.5 TeV, which means the center-of-mass energy was $\sqrt{s} = 13$ TeV. The LHC
¹⁴⁷ machine is described in more technical detail in Ref. [36].

¹⁴⁸ 4.1.1 Luminosity

¹⁴⁹ It depends on several beam parameters. The simplified expression is [10, p. 533]:

$$\mathcal{L} = \frac{N_1 N_2 f}{A}. \quad (4.1)$$

¹⁵⁰ The LHC is designed to reach the nominal luminosity of $\mathcal{L} = 10^{34} \text{ cm}^{-2} \text{ s}^{-1}$. See Fig. 4.2. Each
¹⁵¹ bunch contains about 110 billion protons [36, 38].

¹⁵² Figure 4.4 shows the distribution of the number of interactions per bunch crossing in all

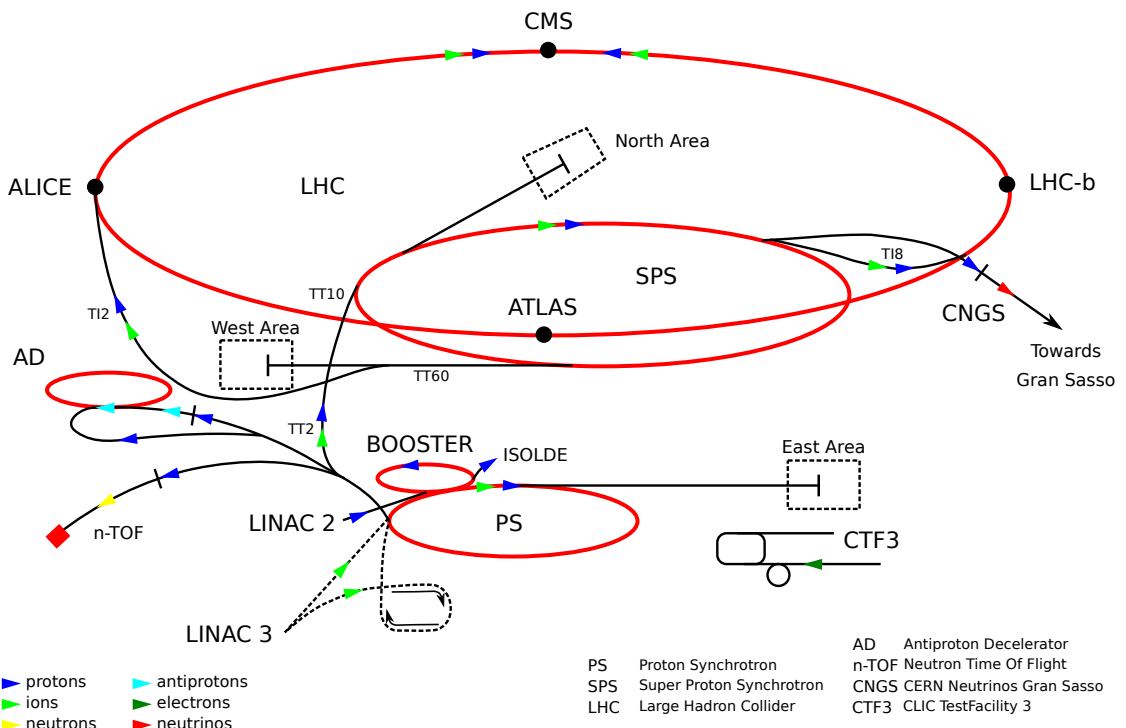


Figure 4.1: CERN's accelerator complex. Taken from [34].

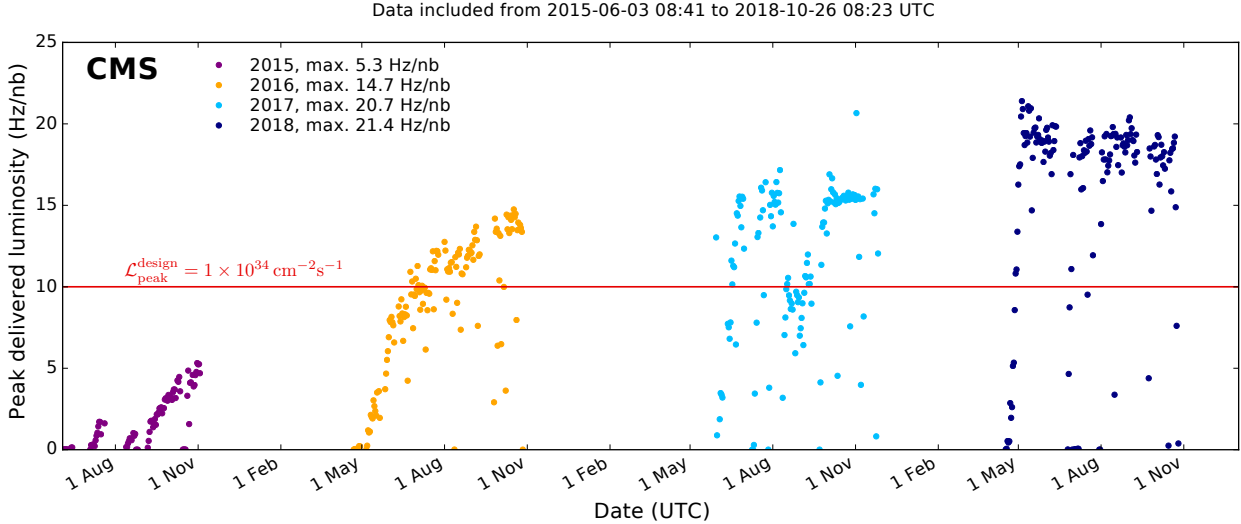


Figure 4.2: The instantaneous luminosity \mathcal{L} . The design luminosity is $\mathcal{L}_{\text{peak}}^{\text{design}} = 10^{34} \text{ cm}^{-2} \text{s}^{-1}$. Adapted from [37].

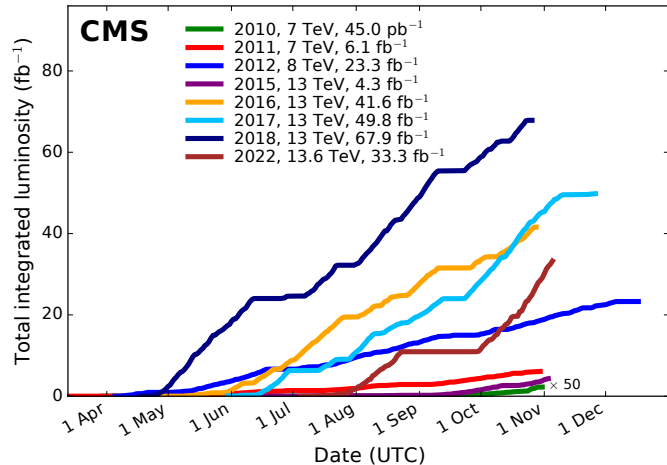


Figure 4.3: Integrated luminosity collected by CMS at $\sqrt{s} = 13 \text{ TeV}$. Figure taken from [37].

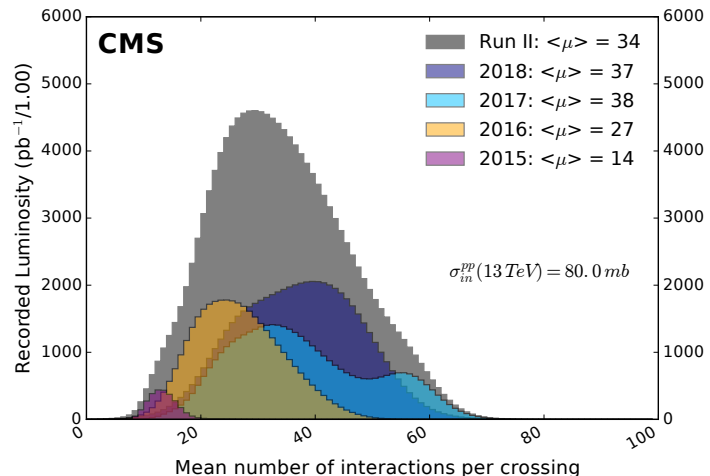


Figure 4.4: Distribution of number of pp interactions, assuming an inelastic cross section of 80 mb. Figure taken from [37].

153 data-taking years of Run 2.

154 Figure 4.3 shows the data of each data-taking year with *integrated luminosity* L , which is

$$L := \int_{\text{data taking}} \mathcal{L}(t) dt, \quad (4.2)$$

155 given in units of inverse area, such as the inverse barn (b^{-1}). Between 2016 and 2018, CMS
156 collected about 138 fb^{-1} of pp collision data for physics analysis.

157 4.2 The CMS detector

158 The Compact Muon Solenoid (CMS) detector at one of the interaction points at the LHC. An
159 illustration is shown in Fig. 4.5. A detailed description can be found in Ref. [39].

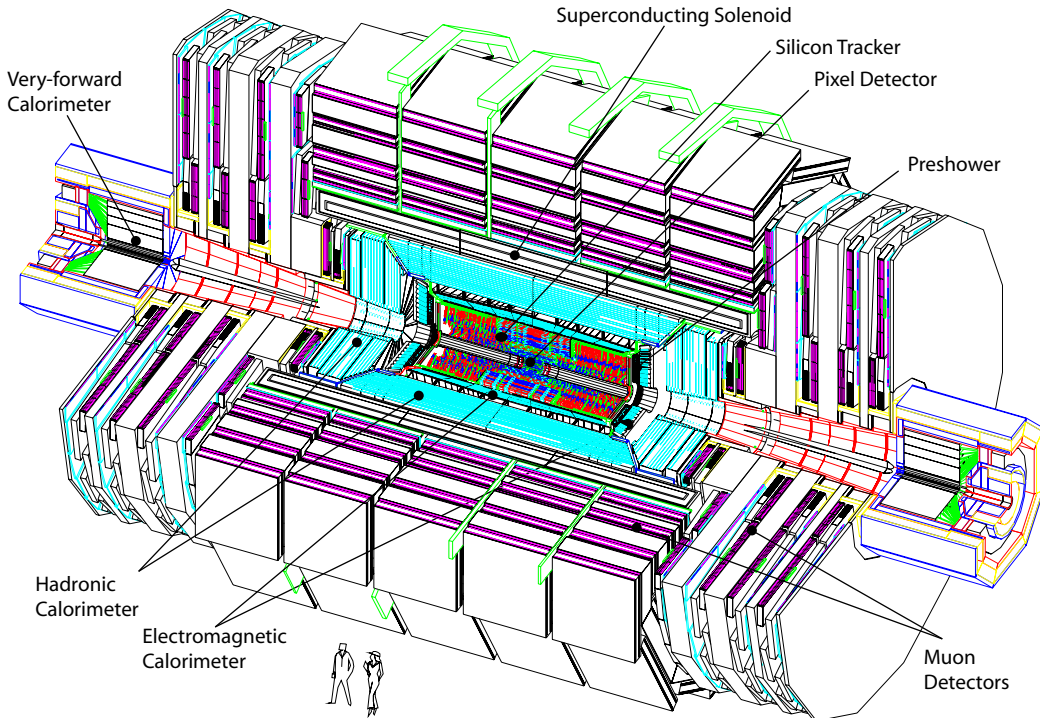


Figure 4.5: The CMS detector. Taken from [39].

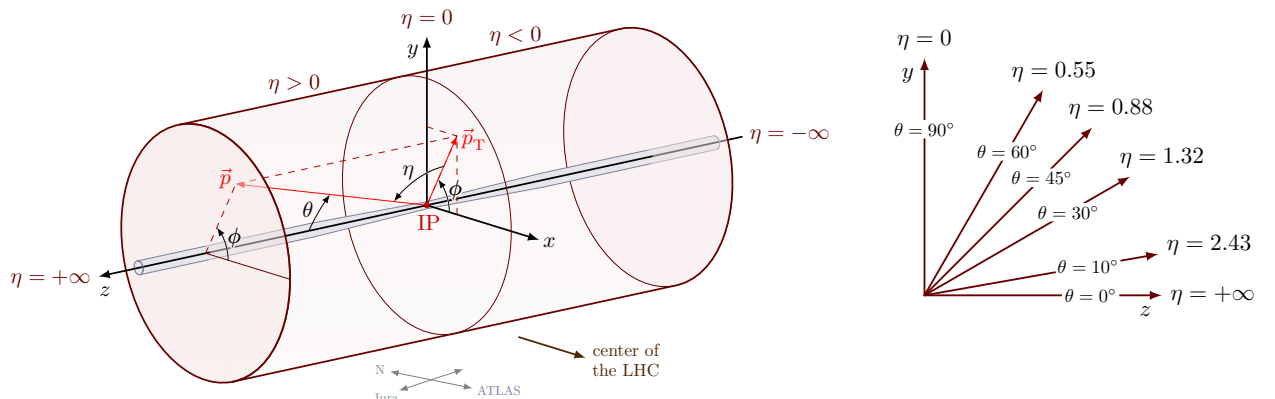


Figure 4.6: Left: The conventional coordinate system of CMS with momentum vector \vec{p} . Taken from [40]. Right: Pseudorapidity. Taken from [41].

160 **4.2.1 Coordinate system**

161 The conventional coordinate system of CMS is defined in Fig. 4.6.

162 **4.2.2 The solenoid magnet & flux-return yoke**

163 The *superconducting solenoid magnet* is a 13 m long cylinder with an inner diameter of 6 m. The
164 yoke [45].

165 **4.2.3 The pixel tracker**

166 The inner tracker system has a *silicon pixel tracker* and a *silicon microstrip tracker*. Figure 4.8
167 presents a closer look of the full tracker layout. The pixel tracker from 2008 up to 2016 was
168 composed of 1440 sensor modules with a total of 66 million silicon pixels [46]. During the
169 technical shutdown it was upgraded with 1856 modules with 124 million pixels in total [44, 47].
170 Their layouts are compared in Fig. 4.9. See Refs. [46, 48] for more information on the resolution.

171 **4.2.4 The silicon strip tracker**

172 The silicon strip tracker is larger. A detailed description of the tracking and vertexing software
173 is given in Ref. [46].

174 **4.2.5 The electromagnetic calorimeter**

175 The *electromagnetic calorimeter* (ECAL) is built around the tracker. The energy resolution can
176 be parametrized as a function of energy [39]:

$$\left(\frac{\sigma_E}{E}\right)^2 = \left(\frac{S}{\sqrt{E}}\right)^2 \oplus \left(\frac{N}{E}\right)^2 \oplus C^2, \quad (4.3)$$

177 with the stochastic term S , the noise N , and a constant term C . The technical design report [49]
178 describes the ECAL in more technical detail.

179 **4.2.6 The hadronic calorimeter**

180 The last subdetector inside the solenoid is the *hadron calorimeter* (HCAL). The jet energy
181 resolution can be found in Ref. [50]

182 The *very forward HCAL* (HF) is positioned around the beamline outside the detector.

183 **4.2.7 The muon system**

184 The muon system is outside the solenoid magnet. The final momentum resolution can be roughly
185 parametrized as follows:

$$\left(\frac{\sigma_{p_T}}{p_T}\right)^2 = (A \cdot p_T)^2 \oplus C^2, \quad (4.4)$$

186 where A , and C are constants determined by the hit resolution and multiple scattering, respec-
187 tively [51]. The resolution grows with momentum, because the track becomes more straight,
188 which increases the uncertainty in its curvature. The technical design report can be found in
189 Ref. [52].

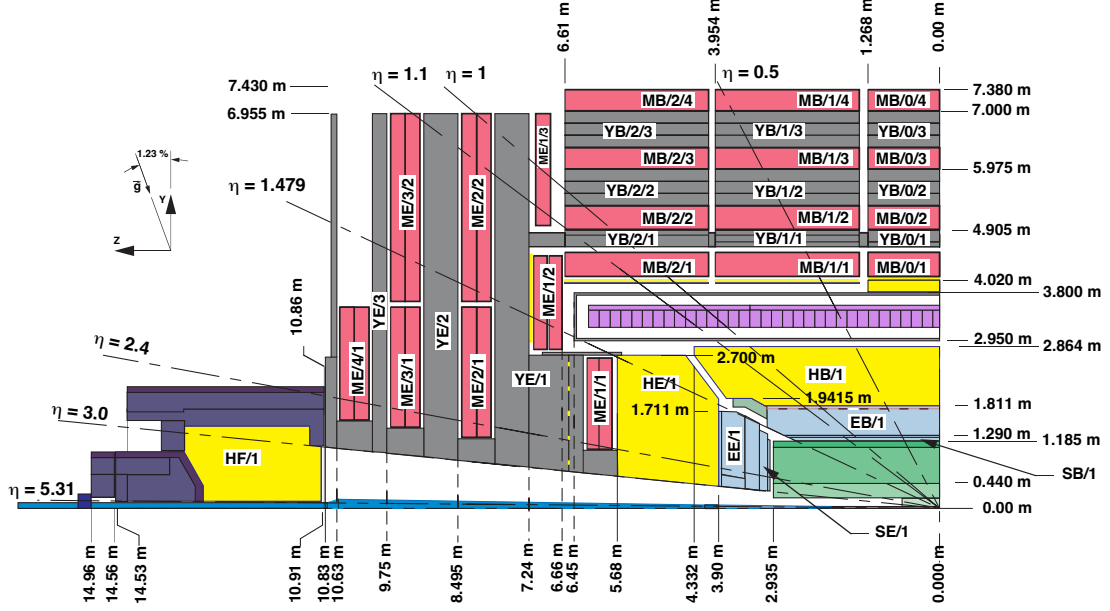


Figure 4.7: Schematic of one quadrant of the CMS detector in the positive zy -plane. Adapted from [42].

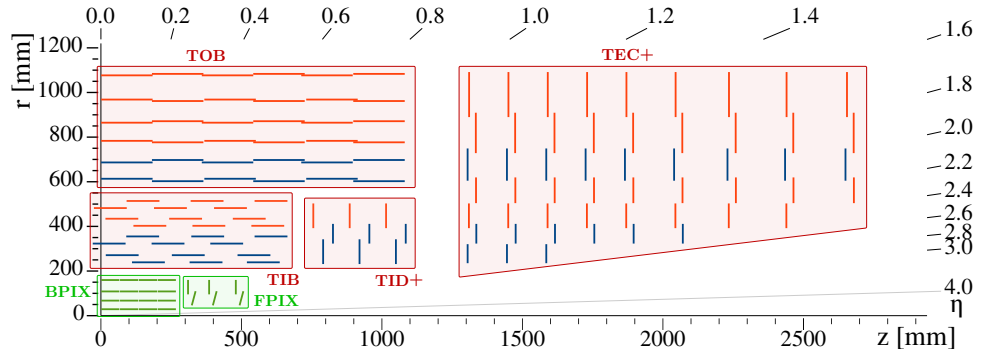


Figure 4.8: Schematic view of the CMS tracking system. Adapted from [43].

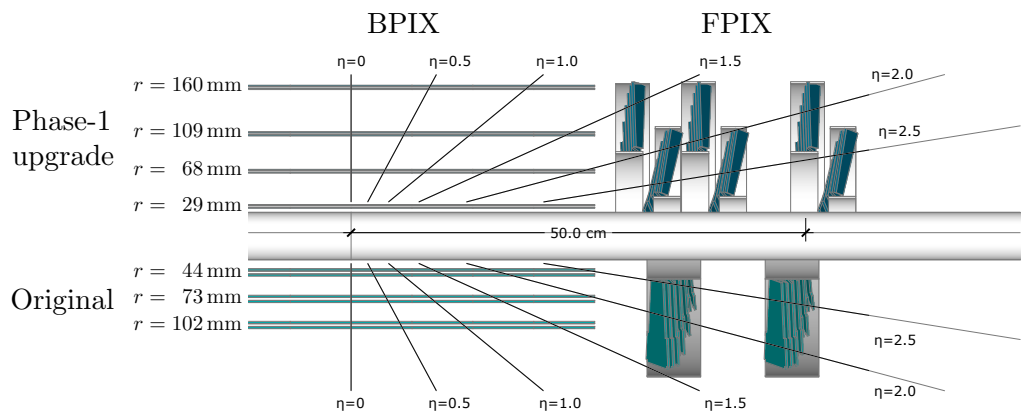


Figure 4.9: Layout of the CMS pixel detector. Adapted from [44].

190 **4.2.8 The trigger system**

191 The collision rate of 40 MHz is higher than is possible to record offline. The *L1 trigger* has a
192 rate of about 100 kHz. The next level, is the *high-level trigger* (HLT). See Ref. [53].

5 Object & Event Reconstruction

193 This chapter explains object and event reconstruction in the CMS experiment.

5.1 Principles of particle identification

196 Figure 5.1 compares the lifetime, dividing them in different regions of stability in the context of
197 the CMS experiment.

198 Each of these particles has a unique set of properties that leave a characteristic signal in one
199 or more of the subdetector, as illustrated in Fig. 5.2.

5.2 Particle-flow algorithm

201 The particle-flow (PF) algorithm [56, 57] fully reconstructs the event of a pp collision with an
202 optimized combination of all measurements of the CMS subsystems.

203 Tracks in the inner tracker or muon system are iteratively built from hits, using the *Kalman-*
204 *filter (KF) technique* [58, 59].

5.3 Primary vertex

206 The algorithm locates primary vertices (PVs) of pp collisions. The tracks are clustered using the
207 *deterministic annealing algorithm* [60]. Finally, candidate vertices are fitted using an *adaptive*
208 *vertex fitter* [61]. The PV with the largest sum of momenta is assumed to be the vertex of the
209 hard scattering process [46, 57, 62].

5.4 Electrons

211 Electrons are reconstructed by associating a track in the inner tracker to clusters of energy
212 deposits in the ECAL. Candidate tracks are refitted with the *Gaussian sum filter* (GSF) [63].
213 The ECAL clusters are recombined into a so-called *supercluster*. The resolution is documented
214 in Ref. [64, 65].

215 The reconstruction and identification of electrons, as well as high-energy photons, are dis-
216 cussed in more detail in Refs. [66] and [64].

217 The *relative isolation* for electrons is computed with the so-called *rho-effective-area method* [67]:

$$I_{\text{rel}}^e := \frac{\sum_{\text{charged}} p_T + \max(0, \sum_{\text{neutral}} E_T - \rho A_{\text{eff}})}{p_T^e}. \quad (5.1)$$

5.5 Muons

219 Muon candidates in CMS are reconstructed as *standalone muons*, *tracker muons*, and/or *global*
220 *muons* [68].

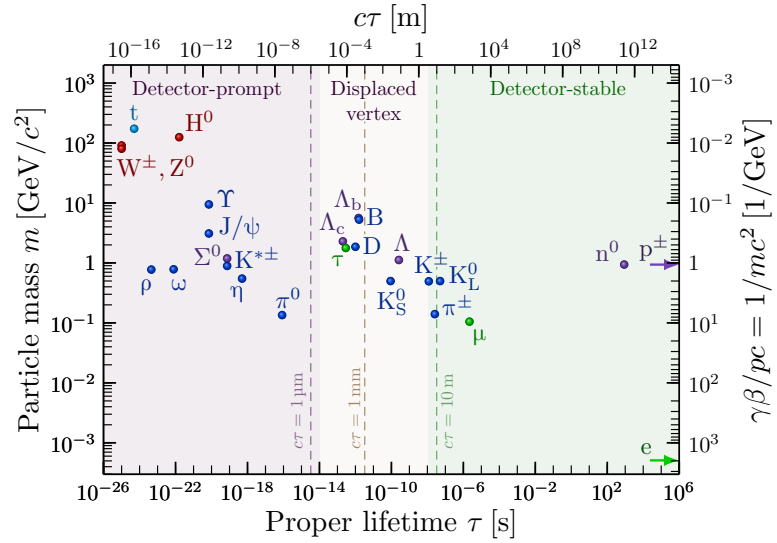


Figure 5.1: Plot of the mass versus lifetime τ of many composite and fundamental SM particles. The decay length is given by $L = \gamma\beta c\tau$, with $\gamma\beta = p/mc$. Adapted from [54].

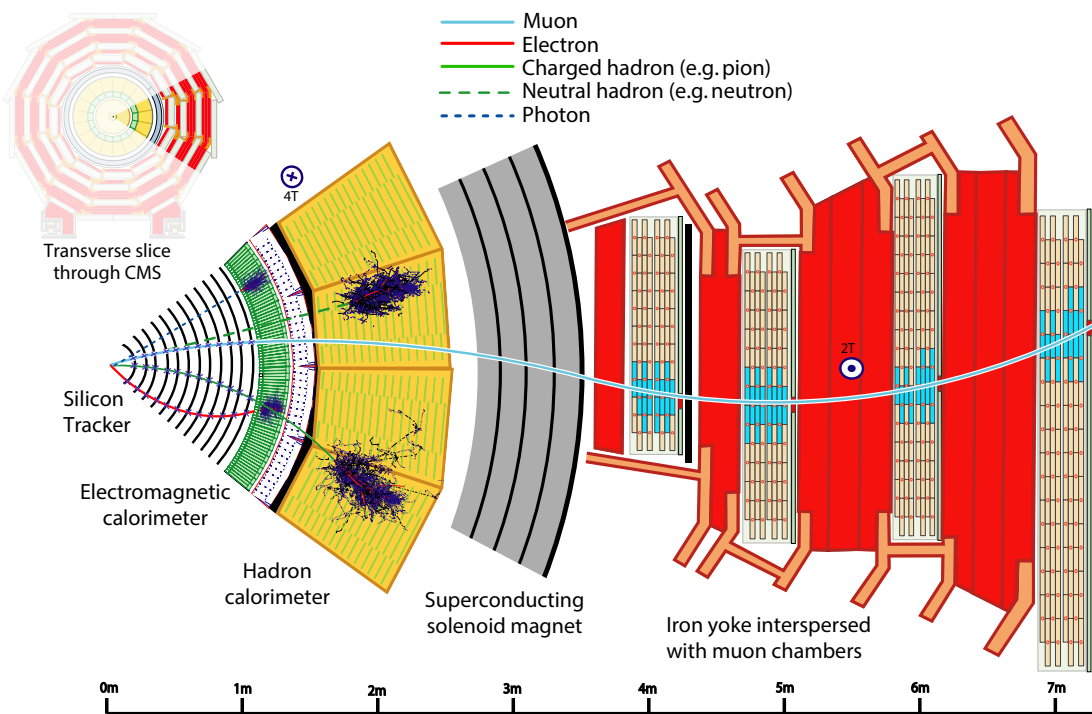


Figure 5.2: Particles in the CMS detector. Adapted from from [55].

221 The relative isolation of a muon is defined with the so-called $\Delta\beta$ -*corrections*:

$$I_{\text{rel}}^{\mu} := \frac{\sum_{\text{charged}} p_T + \max(0, \sum_{\text{neutral}} E_T - \Delta\beta \sum_{\text{charged, PU}} p_T)}{p_T^{\mu}}. \quad (5.2)$$

222 5.6 Hadronically Decayed τ Leptons

223 Hadronic decays of τ leptons (τ_h) are reconstructed with the *hadron-plus-strips* (HPS) *algorithm*
224 [69–72]. About 65% of hadronic τ decays involve neutral pions, which decay promptly ($\tau =$
225 8.4×10^{-17} s) to two photons 98.8% of the time [10, p. 33].

226 The τ_h identification algorithm DEEPTAU [72] was used to discriminate against jets that are
227 initiated by quarks and gluons, as well as electrons and muons, see Fig. 5.5.

228 5.7 Jets

229 Jets are reconstructed with a clustering algorithm. The jet properties must be *infrared safe* and
230 *collinear safe*. The *anti- k_T* (AK) *algorithm* utilizes the metric

$$d_{ij} = \min(p_{T,i}^{-2}, p_{T,j}^{-2}) \frac{\Delta R_{ij}^2}{\Delta R_y^2}, \quad (5.3)$$

231 where $\Delta R_y = \sqrt{\Delta y^2 + \Delta\phi^2}$ is the distance in (y, ϕ) -space with the *rapidity*

$$y := \frac{1}{2} \ln \left(\frac{E + p_z}{E - p_z} \right). \quad (5.4)$$

232 If a cluster i of combined objects satisfies

$$d_{ij} > d_{iB} = p_{T,i}^{-2}, \quad (5.5)$$

233 More info is given in Ref. [57, 75]. The AK algorithm is implemented in the FASTJET library [76,
234 77], and *charged-hadron subtraction* (CHS) is used.

235 The CMS Collaboration determines *jet energy corrections* (JECs) in several steps, which are
236 explained in detail in Ref. [78]. Additionally, the jet energy and *jet energy resolution* (JER) of
237 jets in simulation are corrected to obtain better agreement between simulation and data.

238 Genuine jets are distinguished from pileup jets with the identification algorithm [79]. Iden-
239 tification [80] removes spurious jet-like features that originate from isolated noise patterns in
240 certain HCAL regions.

241 5.8 Bottom quark identification

242 The DEEPCSV algorithm [82, 83] for b tagging jets. DEEPCSV is a deep neural network
243 (DNN) with four hidden layers that is an extension of the combined secondary vertex (CSV)
244 algorithm [82, 83].

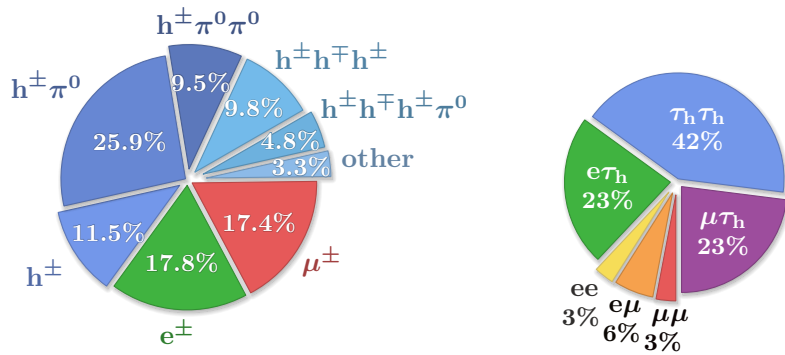


Figure 5.3: Pie charts of branching fractions. **Left:** τ lepton decay. **Right:** Decay channels of a pair of τ leptons. Adapted from Ref. [18]. Numbers from PDG [10, p. 28].

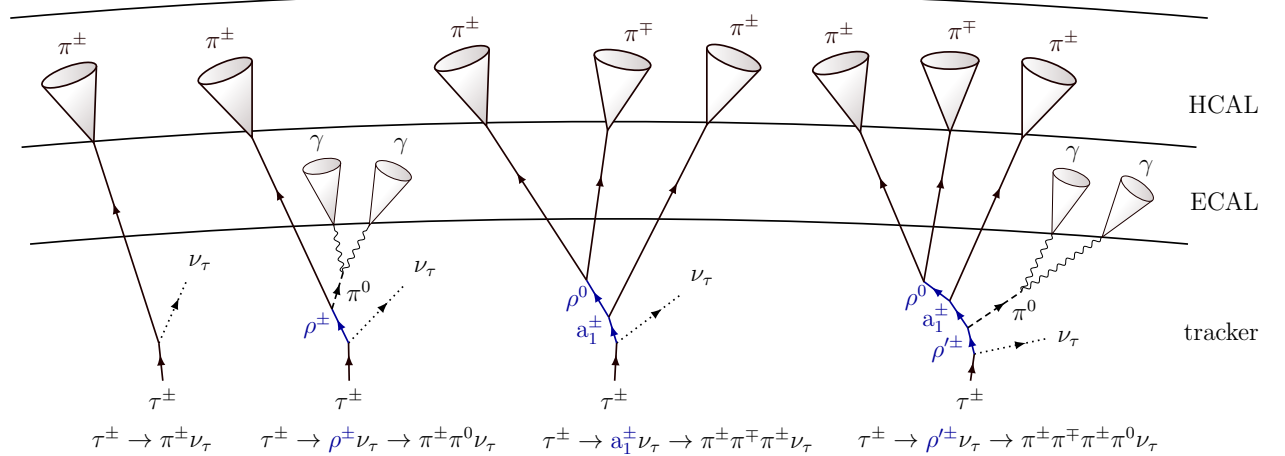


Figure 5.4: An illustration τ_h signatures. Adapted from Ref. [73].

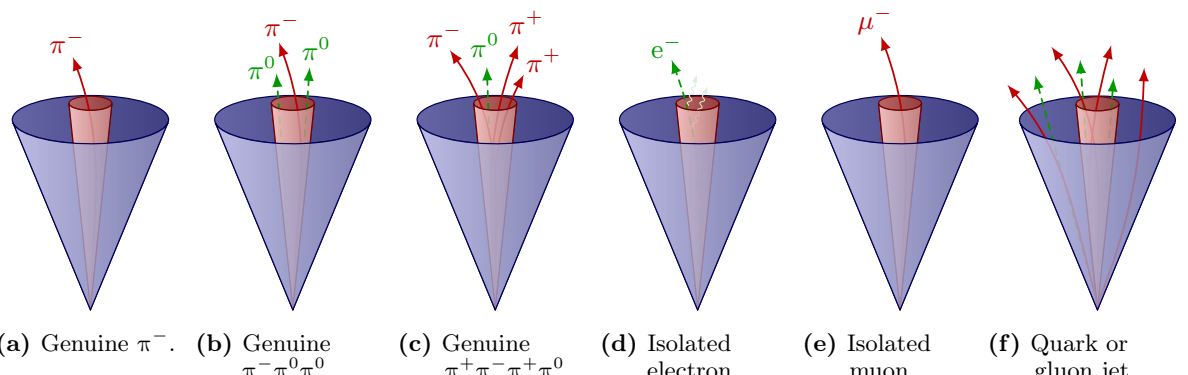


Figure 5.5: Illustration of several hadronic decay modes of the τ leptons (a-c) and their backgrounds (d-f). Adapted from Ref. [74].

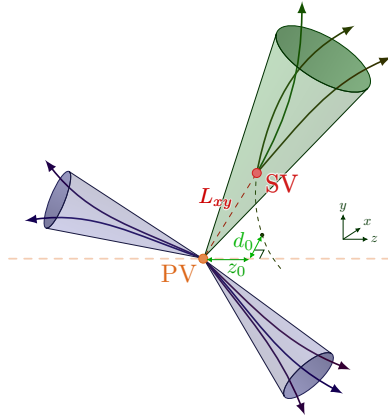


Figure 5.6: B-tagging. Adapted from Ref. [81].

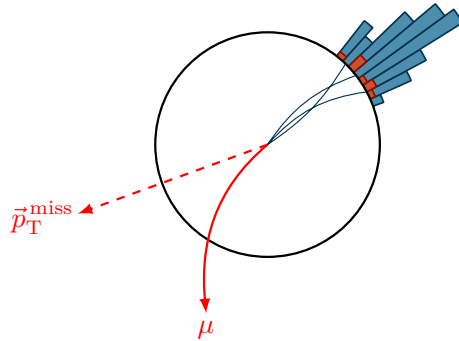


Figure 5.7: Illustration of missing transverse energy (MET) with a muon track (red), and energy deposits in the calorimeters. Adapted from Ref. [84].

245 **5.9 Missing transverse energy**

246 The vectorially sum of all particles gives the missing momentum

$$\vec{p}_T^{\text{miss}} = - \sum_i \vec{p}_T^i. \quad (5.6)$$

247 This vector, or its length, is often referred to as the *missing transverse momentum*, or *missing
248 transverse energy* (MET). Several corrections are applied [57]. More details can be found in
249 Refs. [85] and [86].

250 **6 Data sets & Simulated Samples**

251 This chapter will discuss in more detail the data sets of pp collision events used, as well as the
252 samples of simulated background events.

253 **6.1 Data sets**

254 The total data set recorded between 2016 and 2018 corresponds to an integrated luminosity of
255 approximately 138 fb^{-1} at $\sqrt{s} = 13 \text{ TeV}$. The run ranges and integrated luminosity per year are
256 listed in Table 6.1.

Table 6.1: LHC run number ranges and integrated luminosity L .

Run number range	$L [\text{fb}^{-1}]$
272007–284044	36.3
297020–306462	41.5
315252–325175	59.7

257 **6.2 Event simulation**

258 The PYTHIA parameters affecting the description of the underlying event are set to the CUETP8M1
259 (CP5) tune for all 2016 (2017 and 2018) samples [88, 89], except for the 2016 $t\bar{t}$ sample, for
260 which CUETP8M2T4 [90] is used. The interaction with the CMS detector is simulated by
261 GEANT4 [91]. Pileup is generated with PYTHIA. Event generation is described in more detail in
262 Refs. [10, p. 717], [92] and [93].

263 **6.3 Backgrounds**

264 **6.3.1 Simulated backgrounds**

265 All the simulated background samples used in this thesis are listed in Table 6.2. The $W + \text{jets}$ and
266 $Z + \text{jets}$ processes are generated with MADGRAPH [94] at LO precision. The MLM jet matching
267 and merging scheme [95] is used to match partons between MADGRAPH and PYTHIA and prevent
268 overcounting. The $Z + \text{jets}$ samples generated at NLO by MADGRAPH5_aMC@NLO [96]. The
269 production of $t\bar{t}$ and singly produced top quarks is simulated with the POWHEG [97–99] 2.0 and
270 1.0 generators, respectively, at NLO precision [100–103]. Diboson production is generated at LO
271 with PYTHIA 8 [104, 105]. The NNPDF3.0 PDF sets [106] are used for 2016. The NNPDF3.1
272 PDF [27] sets are used for 2017 and 2018 samples.

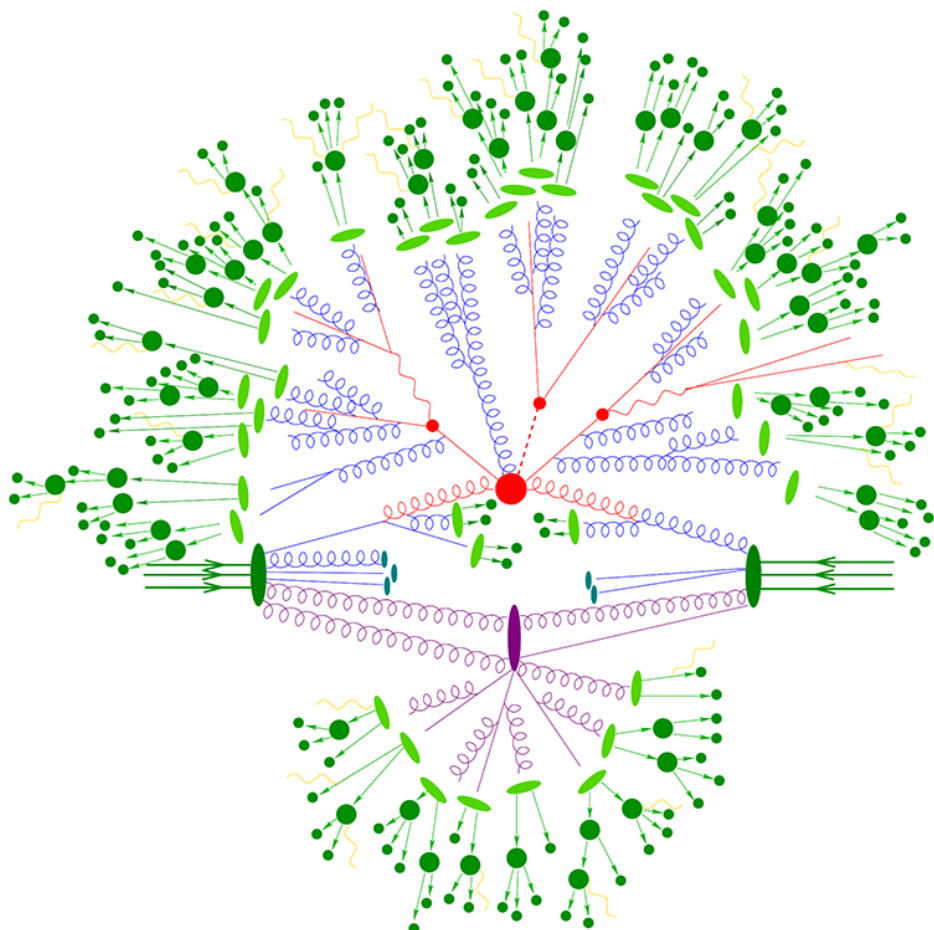


Figure 6.1: Schematic diagram explaining event generation of two colliding protons. Retrieved from [87].

Table 6.2: Summary of simulated SM backgrounds

Process	Generators	Cross section σ [pb]
Drell-Yan, $Z/\gamma^* \rightarrow \ell^+\ell^-$, LO		
+ jets, $10 < m_{\ell\ell} < 50$ GeV	MADGRAPH, PYTHIA	15810.0 (LO), 18610.0 (NLO)
+ jets, $m_{\ell\ell} > 50$ GeV	MADGRAPH, PYTHIA	5343.0 (LO), 6077.2 (NNLO)
+ 1 jets, $m_{\ell\ell} > 50$ GeV	MADGRAPH, PYTHIA	877.8 (LO)
+ 2 jets, $m_{\ell\ell} > 50$ GeV	MADGRAPH, PYTHIA	304.4 (LO)
+ 3 jets, $m_{\ell\ell} > 50$ GeV	MADGRAPH, PYTHIA	111.5 (LO)
+ 4 jets, $m_{\ell\ell} > 50$ GeV	MADGRAPH, PYTHIA	44.05 (LO)
Drell-Yan, $Z/\gamma^* \rightarrow \ell^+\ell^-$, NLO		
+ jets, $m_{\ell\ell} \in [100, 200]$ GeV	aMC@NLO, PYTHIA	247.8 (NLO)
+ jets, $m_{\ell\ell} \in [200, 400]$ GeV	aMC@NLO, PYTHIA	8.502 (NLO)
+ jets, $m_{\ell\ell} \in [400, 500]$ GeV	aMC@NLO, PYTHIA	0.4514 (NLO)
+ jets, $m_{\ell\ell} \in [500, 700]$ GeV	aMC@NLO, PYTHIA	0.2558 (NLO)
+ jets, $m_{\ell\ell} \in [700, 800]$ GeV	aMC@NLO, PYTHIA	0.04023 (NLO)
+ jets, $m_{\ell\ell} \in [800, 1000]$ GeV	aMC@NLO, PYTHIA	0.03406 (NLO)
+ jets, $m_{\ell\ell} \in [1000, 1500]$ GeV	aMC@NLO, PYTHIA	0.01828 (NLO)
+ jets, $m_{\ell\ell} \in [1500, 2000]$ GeV	aMC@NLO, PYTHIA	0.002367 (NLO)
+ jets, $m_{\ell\ell} \in [2000, 3000]$ GeV	aMC@NLO, PYTHIA	5.409×10^{-4} (NLO)
+ jets, $m_{\ell\ell} \in [3000, \infty]$ GeV	aMC@NLO, PYTHIA	3.048×10^{-5} (NLO)
W + jets, $W \rightarrow \ell\nu$		
+ jets	MADGRAPH, PYTHIA	52940.0 (LO), 61526.7 (NLO)
+ 1 jets	MADGRAPH, PYTHIA	8104.0 (LO)
+ 2 jets	MADGRAPH, PYTHIA	2793.0 (LO)
+ 3 jets	MADGRAPH, PYTHIA	992.5 (LO)
+ 4 jets	MADGRAPH, PYTHIA	544.3 (LO)
t̄t + jets		833.9 (NNLO)
Fully leptonic	POWHEG, PYTHIA	88.29 (NNLO), $\mathcal{B} = 10.6\%$
Semi-leptonic	POWHEG, PYTHIA	365.35 (NNLO), $\mathcal{B} = 43.9\%$
Fully Hadronic	POWHEG, PYTHIA	377.96 (NNLO), $\mathcal{B} = 45.4\%$
Single top		
t + W ⁻	POWHEG, PYTHIA	35.85 (NNLO)
̄t + W ⁺	POWHEG, PYTHIA	35.85 (NNLO)
Single t, t channel	POWHEG, PYTHIA	136.02 (NNLO)
Single ̄t, t channel	POWHEG, PYTHIA	80.95 (NNLO)
Diboson		
WW	PYTHIA	75.88 (LO)
WZ	PYTHIA	27.60 (LO)
ZZ	PYTHIA	12.14 (LO)

273 **6.3.2 Cross sections**

274 Table 6.2 also lists the theoretical cross sections σ for each sample. The events are weighted by

$$Z = \frac{L\sigma}{N_{\text{tot}}}, \quad (6.1)$$

275 or with generator weight w_{gen} ,

$$Z = \frac{L\sigma}{\sum w_{\text{gen}}} w_{\text{gen}}. \quad (6.2)$$

276 The LO cross sections of the Z + jets and W + jets samples in Table 6.2 are computed with
277 MADGRAPH. The Z + jets cross section is computed with FEWZ [107] program at NNLO in per-
278 turbative QCD, and with NLO electroweak corrections. The tt}+jets cross section was computed
279 with the TOP++v2.0 program [108, 109] at NNLO and at next-to-next-to-leading logarithmic
280 (NNLL) accuracy. The W + jets production is normalized with cross sections computed at NLO
281 accuracy.

7 Event Selection

This chapter will discuss in more detail the data sets of pp collision events used, as well as the samples of simulated background events.

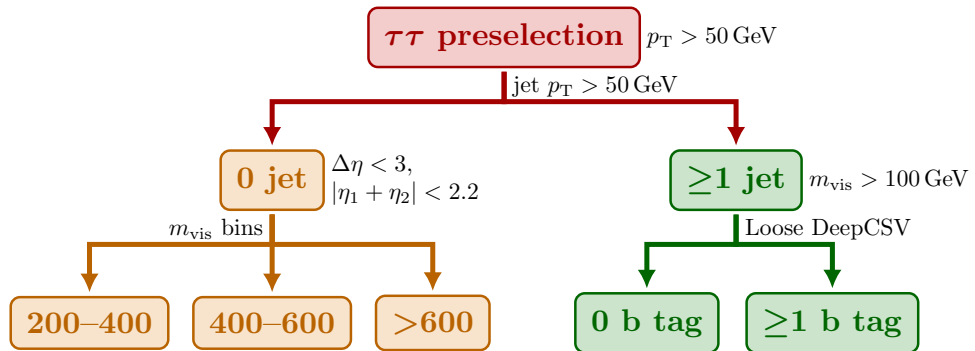


Figure 7.1: Flow chart of event selection.

285 References

- [1] CMS Collaboration, “Observation of a new boson at a mass of 125 GeV with the CMS experiment at the LHC”, *Phys. Lett. B* **716** (2012) 30, doi:10.1016/j.physletb.2012.08.021, arXiv:1207.7235.
- [2] ATLAS Collaboration, “Observation of a new particle in the search for the Standard Model Higgs boson with the ATLAS detector at the LHC”, *Phys. Lett. B* **716** (2012) 1, doi:10.1016/j.physletb.2012.08.020, arXiv:1207.7214.
- [3] CMS Collaboration, “Observation of a new boson with mass near 125 GeV in pp collisions at $\sqrt{s} = 7$ and 8 TeV”, *JHEP* **06** (2013) 081, doi:10.1007/JHEP06(2013)081, arXiv:1303.4571.
- [4] F. Englert and R. Brout, “Broken Symmetry and the Mass of Gauge Vector Mesons”, *Phys. Rev. Lett.* **13** (1964) 321, doi:10.1103/PhysRevLett.13.321.
- [5] P. W. Higgs, “Broken Symmetries and the Masses of Gauge Bosons”, *Phys. Rev. Lett.* **13** (1964) 508, doi:10.1103/PhysRevLett.13.508.
- [6] L. M. Brown, M. Dresden, L. H. Hoddeson, and M. West, eds., “Proceedings, 2nd International Symposium on on the History of Particle Physics in the 1950s: Pions to Quarks: Batavia, USA, May 1-4, 1985”. Univ. Pr., Cambridge, UK, (1989).
- [7] L. H. Hoddeson, L. Brown, M. Riordan, and M. Dresden, eds., “The Rise of the standard model: Particle physics in the 1960s and 1970s. Proceedings, Conference, Stanford, USA, June 24-27, 1992”. (1997).
- [8] D. Griffiths, “Introduction to Elementary Particles”. Wiley-VCH, 2 edition, 2008. ISBN 978-3-527-40601-2.
- [9] Neutelings, Izaak, “History timeline and energy scales – TikZ.net”, <https://tikz.net/timeline/>, 2022. (Retrieved March 26, 2022).
- [10] Particle Data Group, “Review of Particle Physics”, *PTEP* **2022** (2022) 083C01, doi:10.1093/ptep/ptac097.
- [11] ATLAS and CMS Collaborations, “Combined Measurement of the Higgs Boson Mass in pp Collisions at $\sqrt{s} = 7$ and 8 TeV with the ATLAS and CMS Experiments”, *Phys. Rev. Lett.* **114** (2015) 114, doi:10.1103/PhysRevLett.114.191803, arXiv:1503.07589.
- [12] A. Ferrari and N. Rompotis, “Exploration of Extended Higgs Sectors with Run-2 Proton–Proton Collision Data at the LHC”, *Symmetry* **13** (2021), no. 11, 2144, doi:10.3390/sym14081546. [Erratum: Symmetry 14, 1546 (2022)].
- [13] Wikimedia Commons, “File:Standard Model of Elementary Particles.svg — Wikimedia Commons, the free media repository”, https://commons.wikimedia.org/wiki/File:Standard_Model_of_Elementary_Particles.svg, 2023. (Retrieved Jan 13, 2023).
- [14] Neutelings, Izaak, “Standard Model – TikZ.net”, https://tikz.net/sm_particles/,

- 321 2023. (Retrieved Sep 26, 2023).
- 322 [15] G. Isidori, “Lectures notes on Flavour physics”,
 323 <https://www.physik.uzh.ch/en/groups/isidori/teaching.html>, 2016. (Retrieved
 324 Nov 16, 2022).
- 325 [16] Neutelings, Izaak, “Weak hypercharge & isospin – TikZ.net”,
 326 https://tikz.net/sm_isospin_weak/, 2023. (Retrieved Sep 26, 2023).
- 327 [17] S. L. Glashow, J. Iliopoulos, and L. Maiani, “Weak Interactions with Lepton-Hadron
 328 Symmetry”, *Phys. Rev. D* **2** (1970) 1285, doi:10.1103/PhysRevD.2.1285.
- 329 [18] Neutelings, Izaak, “Piechart of SM decays – TikZ.net”,
 330 https://tikz.net/sm_decay_piechart/, 2023. (Retrieved Sep 26, 2023).
- 331 [19] E. D. Bloom et al., “High-Energy Inelastic e^-p Scattering at 6° and 10° ”, *Phys. Rev. Lett.* **23** (1969) 930, doi:10.1103/PhysRevLett.23.930.
- 333 [20] M. Breidenbach et al., “Observed Behavior of Highly Inelastic Electron-Proton
 334 Scattering”, *Phys. Rev. Lett.* **23** (1969) 935, doi:10.1103/PhysRevLett.23.935.
- 335 [21] **ZEUS** and **H1** Collaborations, “Combination of measurements of inclusive deep inelastic
 336 $e^\pm p$ scattering cross sections and QCD analysis of HERA data”, *Eur. Phys. J. C* **75**
 337 (2015), no. 12, 580, doi:10.1140/epjc/s10052-015-3710-4, arXiv:1506.06042.
- 338 [22] R. P. Feynman, “The Behavior of Hadron Collisions at Extreme Energies”, in *High
 339 Energy Collisions: Third International Conference*, p. 237. Stony Brook, N.Y., U.S.A.,
 340 1969.
- 341 [23] J. D. Bjorken and E. A. Paschos, “Inelastic Electron-Proton and γ -Proton Scattering and
 342 the Structure of the Nucleon”, *Phys. Rev.* **185** (1969) 1975,
 343 doi:10.1103/PhysRev.185.1975.
- 344 [24] J. M. Campbell, J. W. Huston, and W. J. Stirling, “Hard Interactions of Quarks and
 345 Gluons: A Primer for LHC Physics”, *Rept. Prog. Phys.* **70** (2007) 89,
 346 doi:10.1088/0034-4885/70/1/R02, arXiv:hep-ph/0611148.
- 347 [25] R. Placakyte, “Parton Distribution Functions”, in *Proceedings, 31st International
 348 Conference on Physics in collisions (PIC 2011)*. Vancouver, Canada, 2011.
 349 arXiv:1111.5452.
- 350 [26] **ALICE** Collaboration, “Parton distributions for the LHC”, *Eur. Phys. J. C* **63** (2009)
 351 189, doi:10.1140/epjc/s10052-009-1072-5, arXiv:0901.0002.
- 352 [27] **NNPDF** Collaboration, “Parton distributions from high-precision collider data”, *Eur.
 353 Phys. J. C* **77** (2017), no. 10, 663, doi:10.1140/epjc/s10052-017-5199-5,
 354 arXiv:1706.00428.
- 355 [28] J. C. Collins and D. E. Soper, “The Theorems of Perturbative QCD”, *Ann. Rev. Nucl.
 356 Part. Sci.* **37** (1987) 383, doi:10.1146/annurev.ns.37.120187.002123.
- 357 [29] J. C. Collins, D. E. Soper, and G. F. Sterman, “Factorization of Hard Processes in
 358 QCD”, *Adv. Ser. Direct. High Energy Phys.* **5** (1989) 11,
 359 doi:10.1142/9789814503266_0001, arXiv:hep-ph/0409313.
- 360 [30] T. Aoyama, M. Hayakawa, T. Kinoshita, and M. Nio, “Tenth-Order QED Contribution

- 361 to the Electron g-2 and an Improved Value of the Fine Structure Constant”, *Phys. Rev.*
 362 *Lett.* **109** (2012) 111807, doi:10.1103/PhysRevLett.109.111807, arXiv:1205.5368.
- 363 [31] T. Aoyama, M. Hayakawa, T. Kinoshita, and M. Nio, “Tenth-Order Electron Anomalous
 364 Magnetic Moment — Contribution of Diagrams without Closed Lepton Loops”, *Phys.*
 365 *Rev. D* **91** (2015), no. 3, 033006,
 366 doi:10.1103/PhysRevD.91.033006, 10.1103/PhysRevD.96.019901, arXiv:1412.8284.
 367 [Erratum: *Phys. Rev. D*96, no.1, 019901 (2017)].
- 368 [32] M. Nio, “QED tenth-order contribution to the electron anomalous magnetic moment and
 369 a new value of the fine-structure constant”, Fundamental Constants Meeting, Eltville,
 370 Germany, 2015. <http://www.bipm.org/cc/CODATA-TGFC/Allowed/2015-02/Nio.pdf>.
- 371 [33] D. Hanneke, S. Fogwell, and G. Gabrielse, “New Measurement of the Electron Magnetic
 372 Moment and the Fine Structure Constant”, *Phys. Rev. Lett.* **100** (2008) 120801,
 373 doi:10.1103/PhysRevLett.100.120801, arXiv:0801.1134.
- 374 [34] L. Forthomme (Wikimedia Commons), “File:Cern-accelerator-complex.svg — Wikimedia
 375 Commons, the free media repository”,
 376 <https://commons.wikimedia.org/wiki/File:Cern-accelerator-complex.svg>, 2016.
 377 (Retrieved Jul 24, 2017).
- 378 [35] S. Holmes, R. S. Moore, and V. Shiltsev, “Overview of the Tevatron Collider Complex:
 379 Goals, Operations and Performance”, *JINST* **6** (2011) T08001,
 380 doi:10.1088/1748-0221/6/08/T08001, arXiv:1106.0909.
- 381 [36] L. Evans and P. Bryant, “LHC Machine”, *JINST* **3** (2008), no. 08, S08001,
 382 doi:10.1088/1748-0221/3/08/S08001.
- 383 [37] CMS Collaboration, “Public CMS Luminosity Information”.
 384 <https://twiki.cern.ch/twiki/bin/view/CMSPublic/LumiPublicResults>. (Retrieved
 385 Dec 6, 2022).
- 386 [38] I. Efthymiopoulos et al., “Bunch Luminosity Variations in LHC Run 2. BUNCH
 387 LUMINOSITY VARIATIONS IN LHC RUN 2”, *JACoW IPAC* **2021** (2021) 4094,
 388 doi:10.18429/JACoW-IPAC2021-THPAB172.
- 389 [39] CMS Collaboration, “The CMS experiment at the CERN LHC”, *JINST* **3** (2008)
 390 S08004, doi:10.1088/1748-0221/3/08/S08004.
- 391 [40] Neutelings, Izaak, “CMS coordinate system – TikZ.net”,
 392 https://tikz.net/axis3d_cms/, 2022. (Retrieved Dec 2, 2022).
- 393 [41] Neutelings, Izaak, “Pseudorapidity – TikZ.net”,
 394 https://tikz.net/axis2d_pseudorapidity/, 2022. (Retrieved Dec 2, 2022).
- 395 [42] CMS Collaboration, “Performance of the CMS Drift Tube Chambers with Cosmic Rays”,
 396 *JINST* **5** (2010) T03015, doi:10.1088/1748-0221/5/03/T03015, arXiv:0911.4855.
- 397 [43] CMS Collaboration, “CMS Tracker Detector Performance Results”,
 398 <https://twiki.cern.ch/twiki/bin/view/CMSPublic/DPGResultsTRK>, 2022.
 399 (Retrieved Dec 2, 2022).
- 400 [44] CMS Tracker Group, “The CMS Phase-1 Pixel Detector Upgrade”, *JINST* **16** (2021),
 401 no. 02, P02027, doi:10.1088/1748-0221/16/02/P02027, arXiv:2012.14304.

- 402 [45] **CMS** Collaboration, “Precise Mapping of the Magnetic Field in the CMS Barrel Yoke
403 using Cosmic Rays”, *JINST* **5** (2015) T03021, doi:10.1088/1748-0221/5/03/T03021,
404 arXiv:0910.5530.
- 405 [46] **CMS** Collaboration, “Description and performance of track and primary-vertex
406 reconstruction with the CMS tracker”, *JINST* **9** (2014) P10009,
407 doi:10.1088/1748-0221/9/10/P10009, arXiv:1405.6569.
- 408 [47] **CMS** Collaboration, “The Phase-1 upgrade of the CMS pixel detector”, *JINST* **12**
409 (2017), no. 07, C07009, doi:10.1088/1748-0221/12/07/C07009.
- 410 [48] **CMS** Collaboration, “CMS Tracking POG Performance Plots For 2017 with PhaseI
411 pixel detector”, [https://twiki.cern.ch/twiki/bin/view/CMSPublic/
412 TrackingPOGPerformance2017MC#Vertex_Resolutions](https://twiki.cern.ch/twiki/bin/view/CMSPublic/TrackingPOGPerformance2017MC#Vertex_Resolutions), 2022. (Retrieved Dec 8, 2022).
- 413 [49] **CMS** Collaboration, “The CMS electromagnetic calorimeter project: Technical Design
414 Report”, Technical Design Report CMS. CERN, Geneva, 1997.
- 415 [50] **CMS** Collaboration, “Jet energy scale and resolution in the CMS experiment in pp
416 collisions at 8 TeV”, *JINST* **12** (2017), no. 02, P02014,
417 doi:10.1088/1748-0221/12/02/P02014, arXiv:1607.03663.
- 418 [51] E. Manca, “Validation of the muon momentum resolution in view of the W mass
419 measurement with the CMS experiment”. PhD thesis, INFN, Pisa, 2016.
420 CMS-TS-2016-024, CERN-THESIS-2016-173.
- 421 [52] **CMS** Collaboration, “The CMS muon project : Technical Design Report”, Technical
422 Design Report CMS. CERN, Geneva, 1997.
- 423 [53] **CMS** Collaboration, “The CMS trigger system”, *JINST* **12** (2017) P01020,
424 doi:10.1088/1748-0221/12/01/P01020, arXiv:1609.02366.
- 425 [54] L. Lee, C. Ohm, A. Soffer, and T.-T. Yu, “Collider Searches for Long-Lived Particles
426 Beyond the Standard Model”, *Prog. Part. Nucl. Phys.* **106** (2019) 210,
427 doi:10.1016/j.ppnp.2019.02.006, arXiv:1810.12602. [Erratum:
428 *Prog.Part.Nucl.Phys.* 122, 103912 (2022)].
- 429 [55] D. Barney, “CMS Slice”, <https://cds.cern.ch/record/2628641/>, 2015. (Retrieved
430 Dec 8, 2022).
- 431 [56] **CMS** Collaboration, “Commissioning of the Particle-flow Event Reconstruction with the
432 first LHC collisions recorded in the CMS detector”, CMS Physics Analysis Summary
433 CMS-PAS-PFT-10-001, CERN, 2010.
- 434 [57] **CMS** Collaboration, “Particle-flow reconstruction and global event description with the
435 CMS detector”, *JINST* **12** (2017) P10003, doi:10.1088/1748-0221/12/10/P10003,
436 arXiv:1706.04965.
- 437 [58] W. Adam, B. Mangano, T. Speer, and T. Todorov, “Track Reconstruction in the CMS
438 tracker”, technical report, CERN, Geneva, 2006.
- 439 [59] R. Fruhwirth, “Application of Kalman filtering to track and vertex fitting”, *Nucl.*
440 *Instrum. Meth. A* **262** (1987) 444, doi:10.1016/0168-9002(87)90887-4.
- 441 [60] K. Rose, “Deterministic annealing for clustering, compression, classification, regression,

- 442 and related optimization problems”, *IEEE Proc.* **86** (1998), no. 11, 2210,
 443 [doi:10.1109/5.726788](https://doi.org/10.1109/5.726788).
- 444 [61] R. Frühwirth, W. Waltenberger, and P. Vanlaer, “Adaptive Vertex Fitting”, technical
 445 report, CERN, Geneva, 2007.
- 446 [62] CMS Collaboration, “Technical proposal for the Phase-II upgrade of the Compact Muon
 447 Solenoid”, CMS Technical Proposal CERN-LHCC-2015-010, CMS-TDR-15-02, CERN,
 448 2015.
- 449 [63] W. Adam, R. Frühwirth, A. Strandlie, and T. Todorov, “Reconstruction of electrons with
 450 the Gaussian-sum filter in the CMS tracker at the LHC”, *Journal of Physics G: Nuclear
 451 and Particle Physics* **31** (2005), no. 9, N9, [doi:10.1088/0954-3899/31/9/n01](https://doi.org/10.1088/0954-3899/31/9/n01).
- 452 [64] CMS Collaboration, “Electron and photon reconstruction and identification with the
 453 CMS experiment at the CERN LHC”, *JINST* **16** (2021) P05014,
 454 [doi:10.1088/1748-0221/16/05/P05014](https://doi.org/10.1088/1748-0221/16/05/P05014), [arXiv:2012.06888](https://arxiv.org/abs/2012.06888).
- 455 [65] CMS Collaboration, “ECAL 2016 refined calibration and Run2 summary plots”, CMS
 456 Detector Performance Summary CMS-DP-2020-021, CERN, 2020.
- 457 [66] CMS Collaboration, “Performance of electron reconstruction and selection with the
 458 CMS detector in proton-proton collisions at $\sqrt{s} = 8$ TeV”, *JINST* **10** (2015) P06005,
 459 [doi:10.1088/1748-0221/10/06/P06005](https://doi.org/10.1088/1748-0221/10/06/P06005), [arXiv:1502.02701](https://arxiv.org/abs/1502.02701).
- 460 [67] M. Cacciari and G. P. Salam, “Pileup subtraction using jet areas”, *Phys. Lett. B* **659**
 461 (2008) 119, [doi:10.1016/j.physletb.2007.09.077](https://doi.org/10.1016/j.physletb.2007.09.077), [arXiv:0707.1378](https://arxiv.org/abs/0707.1378).
- 462 [68] CMS Collaboration, “Performance of the CMS muon detector and muon reconstruction
 463 with proton-proton collisions at $\sqrt{s} = 13$ TeV”, *JINST* **13** (2018) P06015,
 464 [doi:10.1088/1748-0221/13/06/P06015](https://doi.org/10.1088/1748-0221/13/06/P06015), [arXiv:1804.04528](https://arxiv.org/abs/1804.04528).
- 465 [69] CMS Collaboration, “Performance of τ -lepton reconstruction and identification in
 466 CMS”, *JINST* **7** (2012), no. 01, P01001, [doi:10.1088/1748-0221/7/01/P01001](https://doi.org/10.1088/1748-0221/7/01/P01001),
 467 [arXiv:1109.6034](https://arxiv.org/abs/1109.6034).
- 468 [70] CMS Collaboration, “Performance of reconstruction and identification of τ leptons
 469 decaying to hadrons and ν_τ in pp collisions at $\sqrt{s} = 13$ TeV”, *JINST* **13** (2018) P10005,
 470 [doi:10.1088/1748-0221/13/10/P10005](https://doi.org/10.1088/1748-0221/13/10/P10005), [arXiv:1809.02816](https://arxiv.org/abs/1809.02816).
- 471 [71] CMS Collaboration, “Performance of reconstruction and identification of tau leptons in
 472 their decays to hadrons and tau neutrino in LHC Run-2”, CMS Physics Analysis
 473 Summary CMS-PAS-TAU-16-002, CERN, 2016.
- 474 [72] CMS Collaboration, “Identification of hadronic tau lepton decays using a deep neural
 475 network”, *JINST* **17** (2022), no. 07, P07023, [doi:10.1088/1748-0221/17/07/p07023](https://doi.org/10.1088/1748-0221/17/07/p07023),
 476 [arXiv:2201.08458](https://arxiv.org/abs/2201.08458).
- 477 [73] Neutelings, Izaak, “Hadronic tau decay – TikZ.net”, https://tikz.net/tau_decay/,
 478 2023. (Retrieved Sep 26, 2023).
- 479 [74] Neutelings, Izaak, “Hadronic tau decay – TikZ.net”, https://tikz.net/jet_tau/, 2023.
 480 (Retrieved Sep 26, 2023).
- 481 [75] M. Cacciari, G. P. Salam, and G. Soyez, “The anti- k_t jet clustering algorithm”, *JHEP*

- 482 **04** (2008) 063, doi:10.1088/1126-6708/2008/04/063, arXiv:0802.1189.
- 483 [76] M. Cacciari and G. P. Salam, “Dispelling the N^3 myth for the k_T jet-finder”, *Phys. Lett. B* **641** (2006) 57, doi:10.1016/j.physletb.2006.08.037, arXiv:hep-ph/0512210.
- 484 [77] M. Cacciari, G. P. Salam, and G. Soyez, “FastJet user manual”, *Eur. Phys. J. C* **72** (2012) 1896, doi:10.1140/epjc/s10052-012-1896-2, arXiv:1111.6097.
- 485 [78] CMS Collaboration, “Determination of jet energy calibration and transverse momentum resolution in CMS”, *JINST* **6** (2011) P11002, doi:10.1088/1748-0221/6/11/P11002, arXiv:1107.4277.
- 486 [79] CMS Collaboration, “Pileup Jet Identification”, CMS Physics Analysis Summary CMS-PAS-JME-13-005, CERN, 2013.
- 487 [80] CMS Collaboration, “Jet algorithms performance in 13 TeV data”, CMS Physics Analysis Summary CMS-PAS-JME-16-003, CERN, 2017.
- 488 [81] Neutelings, Izaak, “B tagging jets – TikZ.net”, https://tikz.net/jet_btag/, 2023. (Retrieved Sep 26, 2023).
- 489 [82] D. Guest et al., “Jet Flavor Classification in High-Energy Physics with Deep Neural Networks”, *Phys. Rev. D* **94** (2016), no. 11, 112002, doi:10.1103/PhysRevD.94.112002, arXiv:1607.08633.
- 490 [83] CMS Collaboration, “Identification of heavy-flavour jets with the CMS detector in pp collisions at 13 TeV”, *JINST* **13** (2018), no. 05, P05011, doi:10.1088/1748-0221/13/05/P05011, arXiv:1712.07158.
- 491 [84] Neutelings, Izaak, “Transverse plane & missing momentum – TikZ.net”, https://tikz.net/transverse_plane/, 2023. (Retrieved Sep 26, 2023).
- 492 [85] CMS Collaboration, “Performance of missing energy reconstruction in 13 TeV pp collision data using the CMS detector”, CMS Physics Analysis Summary CMS-PAS-JME-16-004, CERN, 2016.
- 493 [86] CMS Collaboration, “Performance of missing transverse momentum in pp collisions at $\sqrt{s} = 13$ TeV using the CMS detector”, CMS Physics Analysis Summary CMS-PAS-JME-17-001, CERN, 2018.
- 494 [87] SLAC Collaboration, “Simulations”. <https://theory.slac.stanford.edu/our-research/simulations>. (Retrieved Jul 25, 2017).
- 495 [88] CMS Collaboration, “Event generator tunes obtained from underlying event and multiparton scattering measurements”, *Eur. Phys. J. C* **76** (2016) 155, doi:10.1140/epjc/s10052-016-3988-x, arXiv:1512.00815.
- 496 [89] CMS Collaboration, “Extraction and validation of a new set of CMS PYTHIA8 tunes from underlying-event measurements”, *Eur. Phys. J. C* **80** (2020) 4, doi:10.1140/epjc/s10052-019-7499-4, arXiv:1903.12179.
- 497 [90] CMS Collaboration, “Investigations of the impact of the parton shower tuning in Pythia 8 in the modelling of $t\bar{t}$ at $\sqrt{s} = 8$ and 13 TeV”, CMS Physics Analysis Summary CMS-PAS-TOP-16-021, CERN, 2016.

- [91] **GEANT4** Collaboration, “GEANT4 — a simulation toolkit”, *Nucl. Instrum. Meth. A* **506** (2003) 250, doi:10.1016/S0168-9002(03)01368-8.
- [92] M. H. Seymour and M. Marx, “Monte Carlo Event Generators”, in *Proceedings, 69th Scottish Universities Summer School in Physics: LHC Phenomenology (SUSSP69) 2012*, p. 287. St.Andrews, Scotland, U.K., 2013. arXiv:1304.6677, doi:10.1007/978-3-319-05362-2_8.
- [93] T. Sjöstrand, S. Mrenna, and P. Z. Skands, “PYTHIA 6.4 Physics and Manual”, *JHEP* **05** (2006) 026, doi:10.1088/1126-6708/2006/05/026, arXiv:hep-ph/0603175.
- [94] F. Maltoni and T. Stelzer, “MadEvent: Automatic event generation with MadGraph”, *JHEP* **02** (2003) 027, doi:10.1088/1126-6708/2003/02/027, arXiv:hep-ph/0208156.
- [95] J. Alwall et al., “Comparative study of various algorithms for the merging of parton showers and matrix elements in hadronic collisions”, *Eur. Phys. J. C* **53** (2008) 473, doi:10.1140/epjc/s10052-007-0490-5, arXiv:0706.2569.
- [96] J. Alwall et al., “The automated computation of tree-level and next-to-leading order differential cross sections, and their matching to parton shower simulations”, *JHEP* **07** (2014) 079, doi:10.1007/JHEP07(2014)079, arXiv:1405.0301.
- [97] P. Nason, “A new method for combining NLO QCD with shower Monte Carlo algorithms”, *JHEP* **11** (2004) 040, doi:10.1088/1126-6708/2004/11/040, arXiv:hep-ph/0409146.
- [98] S. Frixione, P. Nason, and C. Oleari, “Matching NLO QCD computations with parton shower simulations: the POWHEG method”, *JHEP* **11** (2007) 070, doi:10.1088/1126-6708/2007/11/070, arXiv:0709.2092.
- [99] S. Alioli, P. Nason, C. Oleari, and E. Re, “A general framework for implementing NLO calculations in shower Monte Carlo programs: the POWHEG BOX”, *JHEP* **06** (2010) 043, doi:10.1007/JHEP06(2010)043, arXiv:1002.2581.
- [100] S. Frixione, P. Nason, and G. Ridolfi, “A positive-weight next-to-leading-order Monte Carlo for heavy flavour hadroproduction”, *JHEP* **09** (2007) 126, doi:10.1088/1126-6708/2007/09/126, arXiv:0707.3088.
- [101] J. M. Campbell, R. K. Ellis, P. Nason, and E. Re, “Top-Pair Production and Decay at NLO Matched with Parton Showers”, *JHEP* **04** (2015) 114, doi:10.1007/JHEP04(2015)114, arXiv:1412.1828.
- [102] S. Alioli, P. Nason, C. Oleari, and E. Re, “NLO single-top production matched with shower in POWHEG: s - and t -channel contributions”, *JHEP* **09** (2009) 111, doi:10.1088/1126-6708/2009/09/111, arXiv:0907.4076. [Erratum: doi:10.1007/JHEP02(2010)011].
- [103] E. Re, “Single-top Wt-channel production matched with parton showers using the POWHEG method”, *Eur. Phys. J. C* **71** (2011) 1547, doi:10.1140/epjc/s10052-011-1547-z, arXiv:1009.2450.
- [104] T. Sjöstrand, S. Mrenna, and Z. S., Peter, “A Brief Introduction to PYTHIA 8.1”, *Comput. Phys. Commun.* **178** (2008) 852, doi:10.1016/j.cpc.2008.01.036, arXiv:0710.3820.

- 563 [105] T. Sjöstrand et al., “An introduction to PYTHIA 8.2”, *Comput. Phys. Commun.* **191**
564 (2015) 159, doi:10.1016/j.cpc.2015.01.024, arXiv:1410.3012.
- 565 [106] R. D. Ball et al., “Parton distributions for the LHC Run II”, *JHEP* **15** (2015) 40,
566 doi:10.1007/JHEP04(2015)040, arXiv:1410.8849.
- 567 [107] K. Melnikov and F. Petriello, “Electroweak gauge boson production at hadron colliders
568 through O(alpha(s)**2)”, *Phys.Rev. D* **74** (2006) 114017,
569 doi:10.1103/PhysRevD.74.114017, arXiv:hep-ph/0609070.
- 570 [108] M. Czakon and A. Mitov, “Top++: A Program for the Calculation of the Top-Pair
571 Cross-Section at Hadron Colliders”, *Comput. Phys. Commun.* **185** (2014) 2930,
572 doi:10.1016/j.cpc.2014.06.021, arXiv:1112.5675.
- 573 [109] “NNLO+NNLL top-quark-pair cross sections – ATLAS-CMS recommended predictions
574 for top-quark-pair cross sections using the Top++v2.0 program (M. Czakon, A. Mitov,
575 2013)”, <https://twiki.cern.ch/twiki/bin/view/LHCPhysics/TtbarNNLO>, 2022.
576 (Retrieved Dec 21, 2020).